CORTEX 147 (2022) 24–40

Available online at www.sciencedirect.com

ScienceDirect

Journal homepage: www.elsevier.com/locate/cortex

Research Report

Causal dynamics and information flow in parietal-temporal-hippocampal circuits during mental arithmetic revealed by high-temporal resolution human intracranial EEG

Anup Das [a,*] *and Vinod Menon* [a,b,c,**]

[a] *Department of Psychiatry & Behavioral Sciences, Stanford University School of Medicine, Stanford, CA, USA*
[b] *Department of Neurology & Neurological Sciences, Stanford University School of Medicine, Stanford, CA, USA*
[c] *Stanford Neurosciences Institute, Stanford University School of Medicine, Stanford, CA, USA*

ARTICLE INFO

Article history:
Received 6 April 2021
Reviewed 15 July 2021
Revised 19 August 2021
Accepted 11 November 2021
Action editor Paul Reber
Published online 17 December 2021

Keywords:
Human intracranial EEG
Mental arithmetic
Phase transfer entropy
Causal hub
Parietal-temporal-hippocampal circuits

ABSTRACT

Mental arithmetic involves distributed brain regions spanning parietal and temporal cortices, yet little is known about the neural dynamics of causal functional circuits that link them. Here we use high-temporal resolution (1000 Hz sampling rate) intracranial EEG from 35 participants, 362 electrodes, and 1727 electrode pairs, to investigate dynamic causal circuits linking posterior parietal cortex (PPC) with ventral temporal-occipital cortex and hippocampal regions which constitute the perceptual, visuospatial, and mnemonic building blocks of mental arithmetic. Nonlinear phase transfer entropy measures capable of capturing information flow identified dorsal PPC as a causal inflow hub during mental arithmetic, with strong causal influences from fusiform gyrus in ventral temporal-occipital cortex as well as the hippocampus. Net causal inflow into dorsal PPC was significantly higher during mental arithmetic, compared to both resting-state and verbal memory recall. Our analysis also revealed functional heterogeneity of casual signaling in the PPC, with greater net causal inflow into the dorsal PCC, compared to ventral PPC. Additionally, the strength of causal influences was significantly higher on dorsal, compared to ventral, PPC from the hippocampus, and ventral temporal-occipital cortex during mental arithmetic, when compared to both resting-state and verbal memory recall. Our findings provide novel insights into dynamic neural circuits and hubs underlying numerical problem solving and reveal neurophysiological circuit mechanisms by which both the visual number form processing and declarative memory systems dynamically engage the PPC during mental arithmetic.

* *Corresponding author*. Department of Psychiatry & Behavioral Sciences, Stanford University School of Medicine, Stanford, CA, USA.
** *Corresponding author*. Department of Psychiatry & Behavioral Sciences, Stanford University School of Medicine, Stanford, CA, USA.
E-mail addresses: a1das@stanford.edu (A. Das), menon@stanford.edu (V. Menon).
https://doi.org/10.1016/j.cortex.2021.11.012
0010-9452/

A large body of investigations using noninvasive functional magnetic resonance imaging (fMRI) techniques has provided unprecedented insights into the building blocks of numerical cognition in the human brain (Ansari, 2008; Dehaene et al., 2003; Iuculano and Menon, 2018; Menon, 2015; Peters and De Smedt, 2018). While fMRI has been useful for clarifying the functional anatomy of brain areas involved in numerical cognition, its limited temporal resolution precludes precise characterization of dynamic functional circuits that are engaged during problem-solving. Here we use a unique sample of high temporal resolution (1000 Hz sampling rate) intracranial electroencephalography (iEEG) recordings to investigate dynamic causal interactions between multiple parietal and temporal cortical regions which have been implicated in mental arithmetic. A major focus of the present study is the identification of signaling pathways and causal outflow and inflow hubs that link the building blocks of arithmetic problem solving.

Across multiple neuroimaging studies, the posterior parietal cortex (PPC), has been identified as a key brain region for numerical problem solving (Dehaene et al., 2003; Iuculano and Menon, 2018), and impairments in this region are associated with mathematical learning disabilities including acalculia and dyscalculia (Fias et al., 2013; Kucian and von Aster, 2015; Menon et al., 2020). In addition to the PPC, multiple regions in temporal cortex, spanning both its ventral and medial aspects, have also been implicated in numerical problem solving. The ventral temporal-occipital cortex (VTOC), including its inferior temporal cortex and the fusiform gyrus subdivisions, has been implicated in visual perception and identification of numerical symbols (Grotheer et al., 2016a). More recently, the hippocampal subdivision of the medial temporal lobe has also been shown to be important for efficient memory-based retrieval of arithmetic facts and for arithmetic skill acquisition (Bloechle et al., 2016; Cho et al., 2012; Kutter et al., 2018; Moeller et al., 2015; Qin et al., 2014; Supekar et al., 2013). Together, the PPC, VTOC, and hippocampus form crucial building blocks for mental arithmetic and numerical problem solving more broadly. However, the dynamic temporal interactions and information flow between these regions is poorly understood and iEEG studies are needed to determine the electrophysiological properties of causal signaling and hubs linking these brain regions during mental arithmetic.

Convergent with fMRI findings, electrophysiological studies using cortical surface recordings have reported enhanced responses in the intraparietal sulcus and superior parietal lobule within the dorsal PPC, and fusiform gyrus and inferior temporal gyrus (ITG) within the VTOC during mental arithmetic (Daitch et al., 2016; Dastjerdi et al., 2013; Hermes et al., 2017; Pinheiro-Chagas et al., 2018; Vansteensel et al., 2014). Calculation increases activity in the ITG subdivision of the VTOC with a factor of approximately 1.5 during the first 500 msec, whereas no such increases were found for reading numerals without calculation (Hermes et al., 2017). Large concurrent responses have also been reported in surface electrocorticogram recordings in the intraparietal sulcus and superior parietal lobule (Daitch et al., 2016; Hermes et al., 2017; Pinheiro-Chagas et al., 2018). Vansteensel and colleagues examined differences in relative timing of responses and reported earlier responses in occipital areas followed by parietal cortex (Vansteensel et al., 2014). However, dynamic temporal interactions and, specifically, the direction of information flow between PPC and VTOC subdivisions involved in numerical cognition remains unknown. Moreover, due to the lack of adequate electrode placements and participants, involvement of the ventral aspects of the PPC and hippocampus in mental arithmetic has remained unexplored despite emerging findings from fMRI studies of their differential roles in numerical cognition (Bloechle et al., 2016; Cho et al., 2012; Grabner et al., 2009; Qin et al., 2014; Rosenberg-Lee et al., 2011, 2017; Supekar et al., 2013). Furthermore, the ventral PPC and hippocampus are part of default mode network regions involved in semantic and memory processing (Binder & Desai, 2011; Greicius et al., 2003; Schacter et al., 1996). How these distinct PPC regions interact with each other and with the hippocampal regions involved in numerical cognition is largely unknown.

Here we address critical gaps in our knowledge of dynamic causal interactions in key brain areas that have been consistently implicated in numerical cognition. Our study has three main goals. Our first goal was to investigate causal circuits and information flow between key brain regions implicated in numerical cognition. We leveraged iEEG data from the University of Pennsylvania Restoring Active Memory (UPENN-RAM) study (Solomon et al., 2019), consisting of depth recordings from a large number of participants who performed mental arithmetic and verbal memory recall tasks (Fig. 1). We operationalize causality as follows: a brain region has a causal influence on a target if knowing the past history of temporal signals in both regions improves the ability to predict the target's signal in comparison to knowing only the target's past (Granger, 1969; Lobier et al., 2014). We used phase transfer entropy (PTE) (Lobier et al., 2014) which is capable of capturing intermittent and nonstationary causal dynamics observed in iEEG data (Hillebrand et al., 2016; Lobier et al., 2014; Menon et al., 1996). PTE assesses with the ability of one time-series to predict future values of other time-series thus estimating the time-delayed causal influences between the two time-series. Based on its key role in numerical problem solving as identified in fMRI studies, we hypothesized that the dorsal PPC would function as a causal hub in its interaction with other parietal and temporal cortical regions during mental arithmetic. We define causal hubs as follows: A brain region (for example, dorsal PPC) is defined to be a "causal inflow hub" if the net causal inflow PTE(in) − PTE(out) is the maximum among all brain regions. Similarly, a brain region is defined to be a "causal outflow hub" if the net causal outflow PTE(out) − PTE(in) is the maximum among all brain regions.

The second goal of our study was to investigate causal influences of the VTOC and hippocampus on the PPC. Although most previous fMRI research has focused on functional activation and connectivity between VTOC and PPC (Iuculano et al., 2018; Jolles et al., 2016; Moeller et al., 2015; Park et al., 2013), recent studies have revealed an important role of the hippocampus in multiple aspects of numerical cognition including fact retrieval (Chang et al., 2019), identification of symbols corresponding to numerical operations (Mathieu et al., 2018), and efficient problem solving (Cho et al., 2012; Kutter et al., 2018; Moeller et al., 2015; Qin et al., 2014; Supekar et al., 2013). Based on these studies, we tested the hypothesis

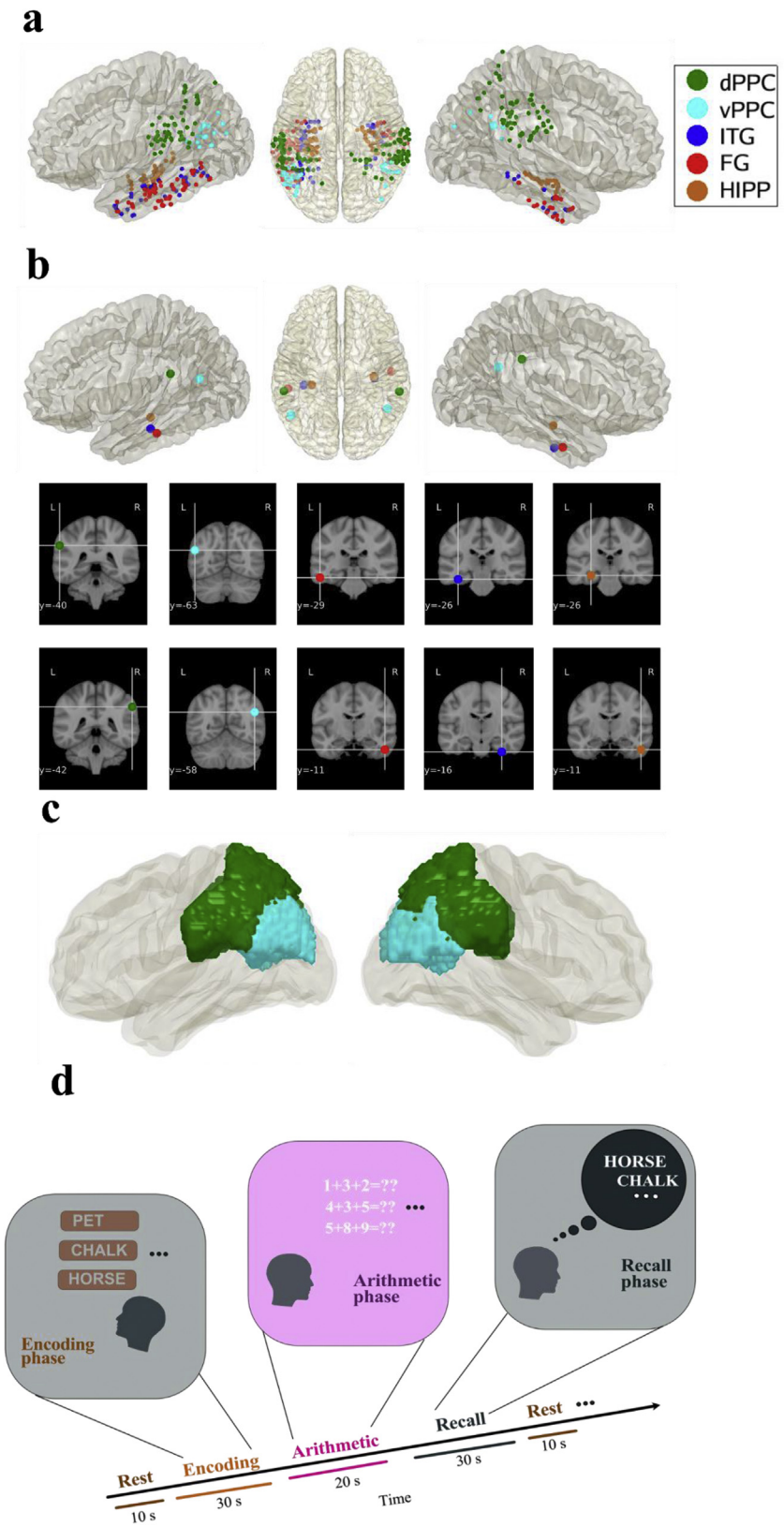

Fig. 1 – Task structure and iEEG recording sites from parietal, temporal, and medial temporal lobe regions investigated in this study. (a) Individual participant iEEG recording sites, (b) Centroids of iEEG recording sites in 3D rendering (top-row), coronal slices of centroids of iEEG recording sites (second and third rows, left and right hemispheres respectively), (c) Surface rendering of the dPPC and vPPC (left column: left hemisphere and right column: right hemisphere), and (d) Task structure. Participants performed multiple trials of a "free recall" experiment. In each trial, they were first presented with a list of words. After the final word, the participants immediately engaged in a series of arithmetic problems of the form *a* +

that the VTOC and hippocampus would have strong causal influences on the PPC, reflecting the perceptual and mnemonic demands of mental arithmetic.

Our third related goal was to contrast the causal dynamics of dorsal and ventral PPC both in relation to causal hubs and specific causal pathways associated with mental arithmetic. Based on differential patterns of activation and deactivation of dorsal and ventral PPC reported in previous fMRI studies (Menon, 2015), as well as reports of ventral PPC involvement in retrieval of arithmetic facts (Grabner et al., 2009, 2013), we hypothesized that the hippocampus and VTOC would show different patterns of causal interaction with dorsal and ventral PPC. Our analysis of information flow reveals causal pathways, hubs, and circuit mechanisms underlying mental arithmetic in the human brain.

1. Results

1.1. Behavioral performance on mental arithmetic task

Thirty-five participants performed a series of arithmetic problems of the form of $a + b + c = ??$, where a, b, and c were randomly selected integers ranging from 1 to 9 during simultaneous iEEG data acquisition (Fig. 1, Methods). Participants were instructed to complete as many problems as possible within a ~20 sec time window. Mean accuracy was 93.23% ± 4.69% and the median reaction time was 5.88 sec ± .49 sec, indicating that participants performed the task with a high level of accuracy.

1.2. Directed information flow during mental arithmetic

We investigated dynamic causal interactions between multiple subdivisions of the PPC and VTOC and the hippocampus. Based on availability of sufficient electrode pairs in five or more study participants (see Methods), we demarcated two distinct subdivisions in the PPC: a dorsal PPC region encompassing the intraparietal sulcus, superior parietal lobule, and supramarginal gyrus and the ventral PPC encompassing the angular gyrus. This choice was further motivated by the different functional roles ascribed to dorsal PPC and the angular gyrus in mental arithmetic as noted above (Daitch et al., 2016; Dastjerdi et al., 2013; Hermes et al., 2017; Pinheiro-Chagas et al., 2018; Vansteensel et al., 2014). Using a similar strategy, we demarcated inferior temporal gyrus (ITG) and fusiform gyrus (FG) subdivisions of the VTOC encompassing its medial and lateral aspects.

Time series from electrode pairs in the dorsal PPC, ventral PPC, ITG, FG, and the hippocampus were then used to examine directed information flow using PTE (Lobier et al., 2014), which provides a robust estimation of directed information flow (Methods, Tables 1–4, Fig. 1a, b, c, d). Visualization of the strength of directed information flow between these regions suggests that the dorsal PPC is distinguished from other brain regions as having higher inflow than outflow (Fig. 2a). To further visualize the pattern of causal interactions, we examined the top 50% of all causal connections between dorsal PPC, ventral PPC, ITG, FG, and hippocampus during mental arithmetic. We found that the strongest causal connections of dorsal PPC are all inflow links, whereas causal connections for ventral PPC, ITG, FG, and hippocampus are either outflow links or bidirectional, during mental arithmetic (Fig. 2b).

We next sought to quantify net outflow and inflow for each node from each of the other four brain areas. Specifically, we computed the outflow of each region, defined as the sum of PTE from electrodes in one brain area to electrodes in the other four brain areas, and the inflow as the reverse. The difference between inflow and outflow was used to determine the inflow hub. This analysis identified dorsal PPC as the region with the strongest inflow during mental arithmetic ($p < .05$, linear mixed effects, FDR corrected for multiple comparisons; Fig. 2c).

Table 1 – Participant demographic information.

Participant ID	Gender	Age
184	M	42
185	M	20
186	M	27
187	F	51
189	M	22
193	M	37
195	M	44
196	M	18
200	M	25
202	F	29
203	F	36
204	F	25
207	F	39
215	F	50
222	F	20
223	F	42
228	F	58
230	F	56
232	M	27
234	M	25
236	F	51
240	F	37
247	F	61
251	M	31
260	F	57
264	F	52
268	F	32
275	M	41
283	F	29
286	F	57
292	F	39
297	M	24
298	F	24
299	M	43
310	M	20

$b + c = ??$, with a, b, and c representing randomly selected integers ranging from 1 to 9. After the completion of the final arithmetic problem, the participants were asked to recall as many words as possible from the original list (see Methods for details). dPPC: dorsal posterior parietal cortex, vPPC: ventral posterior parietal cortex, ITG: inferior temporal gyrus, FG: fusiform gyrus, HIPP: hippocampus.

Table 2 – Brainnetome subregions according to Brodmann areas included in each ROI. dPPC: dorsal posterior parietal cortex, vPPC: ventral posterior parietal cortex, ITG: inferior temporal gyrus, FG: fusiform gyrus, HIPP: hippocampus.

dPPC
A7r, rostral area 7
A7c, caudal area 7
A5l, lateral area 5
A7pc, postcentral area 7
A7ip, intraparietal area 7(hIP3)
A39rd, rostrodorsal area 39(Hip3)
A40rd, rostrodorsal area 40(PFt)
A40c, caudal area 40(PFm)
A40rv, rostroventral area 40(PFop)
vPPC
A39c, caudal area 39(PGp)
A39rv, rostroventral area 39(PGa)
ITG
A20iv, intermediate ventral area 20
A37elv, extreme lateroventral area37
A20r, rostral area 20
A20il, intermediate lateral area 20
A37vl, ventrolateral area 37
A20cl, caudolateral of area 20
A20cv, caudoventral of area 20
FG
A20rv, rostroventral area 20
A37mv, medioventral area37
A37lv, lateroventral area37
Hippocampus
rHipp, rostral hippocampus
cHipp, caudal hippocampus

To determine brain regions that exert the strongest causal influences on the dorsal PPC, we compared causal inflow into dorsal PPC from other parietal and temporal lobe regions (ventral PPC, ITG, FG, and hippocampus) during mental arithmetic. Our analysis revealed that hippocampus has the strongest causal influence on the dorsal PPC, followed by FG (*ps* < .05, linear mixed effects, FDR corrected for multiple comparisons; Fig. 2d).

1.3. *Directed information flow from temporal lobe to PPC during mental arithmetic*

Next, to assess whether temporal lobe regions show differential causal connections with dorsal and ventral PPC, we directly compared causal inflow from temporal lobe regions (ITG, FG, and hippocampus) into dorsal versus ventral PPC during mental arithmetic. Causal inflow from ITG and FG, but not from hippocampus, into dorsal PPC was higher than into ventral PPC (*ps* < .05, linear mixed effects, FDR corrected for multiple comparisons; Fig. 3). This result suggests that the VTOC interacts more strongly with the dorsal PPC during mental arithmetic.

1.4. *Directed information flow during mental arithmetic, compared to resting-state and verbal memory recall*

Next, we sought to assess task-dependent causal influences on the dorsal PPC, we compared the net causal inflow between mental arithmetic, resting-state, and verbal memory recall conditions. This analysis revealed that the net causal inflow into dorsal PPC was higher during mental arithmetic, compared to resting-state ($p < .001$) and verbal memory recall conditions ($p < .001$, linear mixed effects, FDR corrected for multiple comparisons; Fig. 4a). In contrast, the net causal inflow into ventral PPC did not differ between mental arithmetic and resting-state ($p > .05$), and was higher during verbal memory recall compared to mental arithmetic ($p < .05$, linear mixed effects, FDR corrected for multiple comparisons; Fig. 4b). These results suggest that stronger causal inflow into dorsal PPC was observed during mental arithmetic, compared to both resting state and verbal memory recall, whereas ventral PPC showed undifferentiated profiles of causal interactions between mental arithmetic and resting-state and enhanced net causal inflow during verbal memory recall compared to mental arithmetic.

1.5. *Surrogate data analysis of causal information flow between brain regions*

Next, we conducted surrogate data analysis to test the significance of the estimated PTE values compared to PTE

Table 3 – Number of electrode pairs used in inter-network connectivity analysis. dPPC: dorsal posterior parietal cortex, vPPC: ventral posterior parietal cortex, ITG: inferior temporal gyrus, FG: fusiform gyrus, HIPP: hippocampus.

Network pairs	Number of electrode pairs[a] (n)	Number of participants	Participant IDs
ITG-FG	366	12	185, 223, 230, 234, 236, 240, 264, 268, 283, 297, 298, 299
ITG-vPPC	89	6	195, 230, 232, 240, 260, 299
ITG-dPPC	318	10	195, 204, 232, 234, 236, 240, 260, 268, 297, 299
ITG-HIPP	199	12	195, 223, 230, 236, 240, 264, 268, 283, 297, 298, 299, 310
FG-vPPC	49	5	186, 196, 230, 240, 299
FG-dPPC	142	8	186, 196, 234, 236, 240, 268, 297, 299
FG-HIPP	141	10	223, 230, 236, 240, 264, 268, 283, 297, 298, 299
vPPC-dPPC	239	11	184, 186, 193, 195, 196, 203, 232, 240, 260, 275, 299
vPPC-HIPP	64	6	195, 203, 230, 240, 275, 299
dPPC-HIPP	120	10	195, 203, 236, 240, 247, 268, 275, 292, 297, 299

[a] For subject 193, the math epochs did not meet the selection criteria (see Methods for details). The number of electrode pairs (n) for the math task was 206 for vPPC-dPPC interaction.

Table 4 – Centroid of electrodes in each brain region. dPPC: dorsal posterior parietal cortex, vPPC: ventral posterior parietal cortex, ITG: inferior temporal gyrus, FG: fusiform gyrus, HIPP: hippocampus, (L)-left hemisphere, (R)-right hemisphere.

Brain region	Centroid (in MNI coordinates)
ITG (L)	−53.8, −29.9, −19.4
ITG (R)	50.5, −11.2, −31.0
FG (L)	−37.8, −26.3, −21.9
FG (R)	33.5, −16.7, −34.6
dPPC (L)	−58.0, −40.4, 32.4
dPPC (R)	58.6, −42.2, 37.7
vPPC (L)	−50.6, −63.6, 24.7
vPPC (R)	46.4, −58.5, 29.3
HIPP (L)	−29.8, −26.4, −15.8
HIPP (R)	32.9, −17.5, −18.1

expected by chance (Methods). The estimated phases from the Hilbert transform for electrodes from pairs of brain areas were time-shuffled and PTE analysis was repeated on this shuffled data to build a distribution of surrogate PTE values against which the observed PTE was tested. This analysis revealed that causal information flow between all, but one (dPPC→FG), pairs of brain regions were significantly higher than those expected by chance in broadband during mental arithmetic ($p < .05$; Fig. 5). These results demonstrate that reported effects in this study arise from causal signaling that is significantly enhanced above chance levels.

1.6. *Broadband power in dorsal PPC and other parietal and temporal regions during mental arithmetic*

Next, to determine whether the observed causal dynamics of dorsal PPC during mental arithmetic was driven by differences in the amplitude of iEEG fluctuations between brain regions, we compared broadband power across dorsal PPC, ventral PPC, ITG, FG, and hippocampus (see Methods for details; also see Fig. 6 for spectrogram showing time-frequency resolved broadband power). This analysis revealed that broadband power in dorsal PPC did not differ from that in other brain regions during mental arithmetic ($ps > .05$, linear mixed effects, FDR corrected for multiple comparisons). These results suggest that the causal dynamics of dorsal PPC during mental arithmetic are not driven by iEEG amplitude fluctuations.

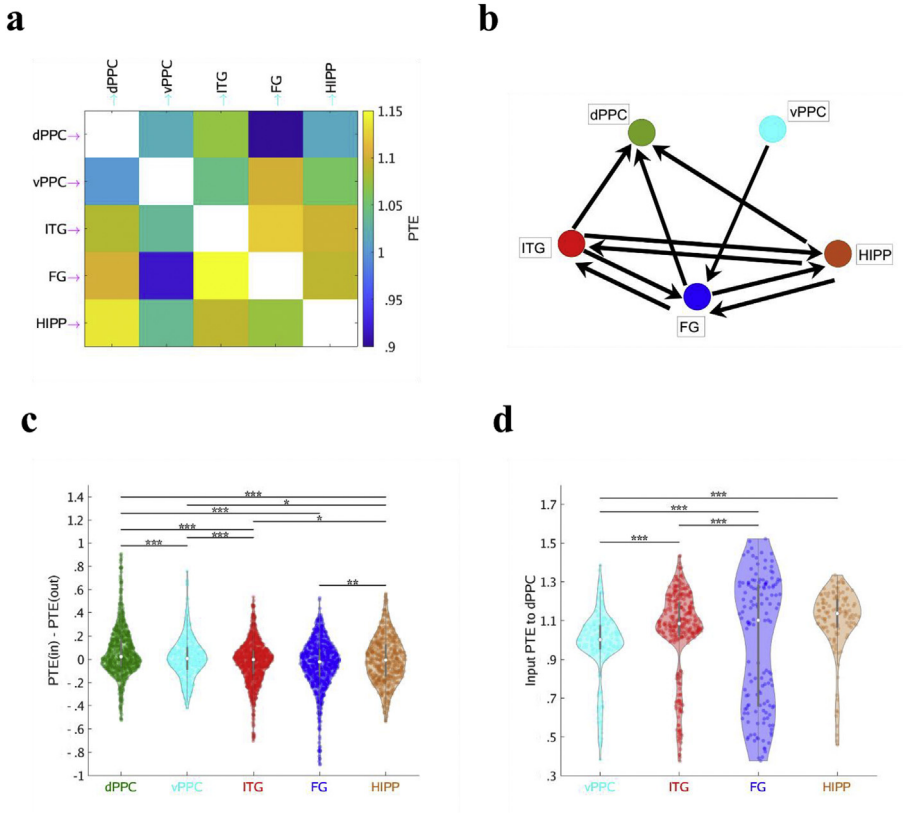

Fig. 2 – Dynamic causal network interactions, measured using phase transfer entropy (PTE, in bits), during mental arithmetic. (a) Matrix representation of causal inflow to (X-axis, cyan arrows) and outflow from (Y-axis, magenta arrows) all brain regions considered in this study. The dorsal posterior parietal cortex (dPPC) is distinguished from other brain regions as having higher PTE(in) than PTE(out). (b) Visualization of the top 50% causal connections showing pathways contributing to strong differential inflow into the dPPC. (c) The dPPC is a causal inflow hub. (d) Comparison of causal inflow into dPPC from other parietal and temporal lobe regions. The strongest causal influence on the dPPC was from the hippocampus (HIPP), followed by the FG. ***$p < .001$, *$p < .05$ (two-way ANOVA, FDR-corrected for multiple comparisons). vPPC: ventral posterior parietal cortex.

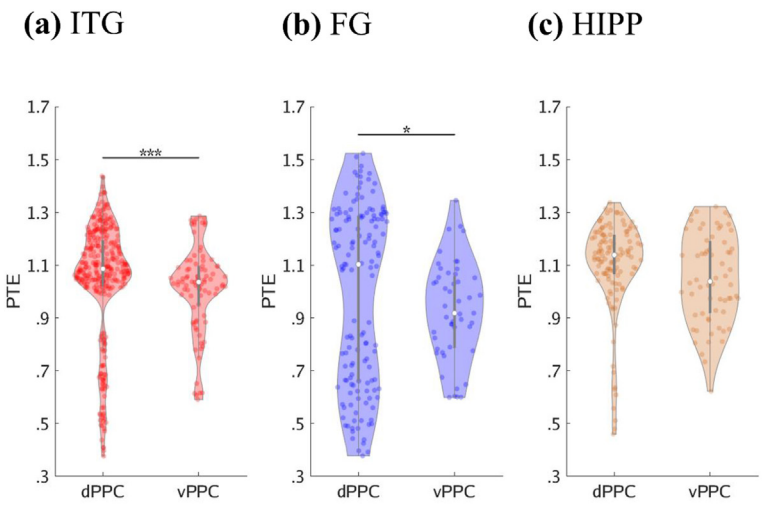

Fig. 3 – Comparison of causal inflow into dorsal versus ventral posterior parietal cortex during mental arithmetic. Causal inflow into the dorsal posterior parietal cortex (dPPC) was higher than into ventral posterior parietal cortex (vPPC) from both the ITG and FG, but not HIPP. ***$p < .001$, *$p < .05$ (two-way ANOVA, FDR-corrected for multiple comparisons).

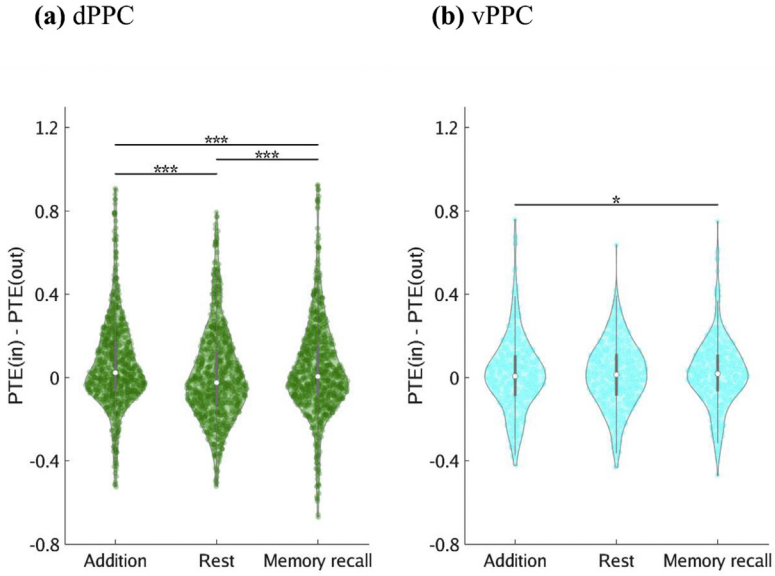

Fig. 4 – Comparison of net causal inflow into (a) dorsal PPC and (b) ventral PPC during mental arithmetic, resting-state, and memory recall. The dorsal PPC (dPPC) is a stronger causal inflow hub during mental arithmetic, compared to both resting-state and memory recall. In contrast, net causal inflow of the ventral PPC (vPPC) during the mental arithmetic did not differ from resting-state and was lower than that during memory recall. ***$p < .001$, *$p < .05$ (two-way ANOVA, FDR-corrected for multiple comparisons).

1.7. *High-gamma band power and causal dynamics of dorsal PPC during mental arithmetic*

Previous studies have suggested that power in the high-gamma band (80–160 Hz) is correlated with fMRI BOLD signals (Schölvinck et al., 2010), and is thought to reflect inputs into a specific brain region (Canolty & Knight, 2010). We compared high-gamma band power (see Methods for details) during mental arithmetic across the ROIs. This analysis revealed that high-gamma power in dorsal PPC did not differ from that in other brain regions during mental arithmetic (*ps* > .05, linear mixed effects, FDR corrected for multiple comparisons). This result suggests that the causal dynamics of dorsal PPC during mental arithmetic are not driven by higher high-gamma power in dorsal PPC electrodes compared to electrodes in other brain regions.

1.8. *Power in dorsal PPC during mental arithmetic, resting-state, and verbal memory recall*

Finally, to determine whether differential causal dynamics of dorsal PPC during mental arithmetic, compared to resting-state and verbal memory recall, were driven by differences in the amplitude of iEEG fluctuations, we compared power (see

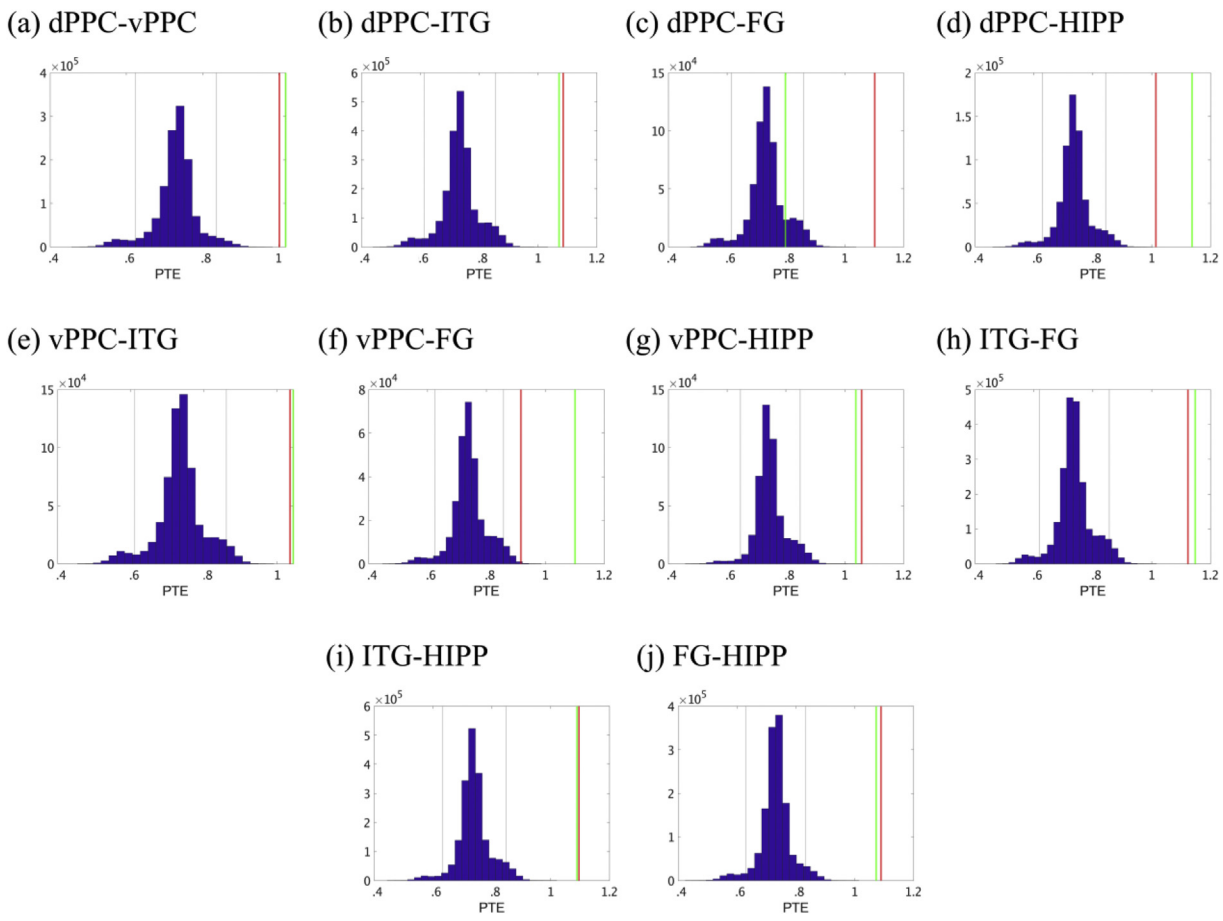

Fig. 5 – Surrogate data analysis to test the statistical significance of the observed PTE values for each pair of brain regions compared to those obtained by chance during mental arithmetic in broadband. (a) vPPC → dPPC (red) and dPPC → vPPC (green). (b) ITG → dPPC (red) and dPPC → ITG (green). (c) FG → dPPC (red) and dPPC → FG (green). (d) dPPC → HIPP (red) and HIPP → dPPC (green). (e) ITG → vPPC (red) and vPPC → ITG (green). (f) FG → vPPC (red) and vPPC → FG (green). (g) vPPC → HIPP (red) and HIPP → vPPC (green). (h) ITG → FG (red) and FG → ITG (green). (i) ITG → HIPP (red) and HIPP → ITG (green). (j) FG → HIPP (red) and HIPP → FG (green). The estimated phases from the Hilbert transform for a given pair of brain areas were time-shuffled and PTE analysis was repeated on this shuffled data to build a distribution of surrogate PTE values against which the observed PTE was tested ($p < .05$). Black lines in all plots denote the $p = .05$ threshold.

Methods for details) in dorsal PPC during mental arithmetic with resting-state and verbal memory recall. This analysis revealed that power in dorsal PPC during mental arithmetic did not differ from resting-state and verbal memory recall in all except one (power during memory recall was higher than power during mental arithmetic in broadband, $p < .05$) condition in both broadband ($ps > .05$, linear mixed effects, FDR corrected for multiple comparisons) and the high-gamma band ($ps > .05$, linear mixed effects, FDR corrected for multiple comparisons). The distinct causal dynamics of dorsal PPC during mental arithmetic, compared to resting-state and verbal memory recall, is therefore not likely driven by differences in the amplitude of iEEG fluctuations.

2. Discussion

iEEG is a particularly useful tool for probing information flow and dynamics of causal interactions associated with distributed brain regions involved in problem solving. This study addresses crucial gaps in our knowledge of parietal-temporal-hippocampal circuit dynamics underlying mental arithmetic using depth iEEG recordings from the UPENN-RAM study (Solomon et al., 2019) and a large sample of 35 participants, 362 electrodes, and 1727 electrode pairs. Our analysis revealed distinct patterns of information flow between dorsal PPC, ventral PPC, VTOC, and the hippocampus which together constitute key multicomponent processing nodes for mental arithmetic in the human brain (Menon et al., 2020). The dorsal PPC emerged as a causal inflow hub during mental arithmetic with significant information flow from both the VTOC and hippocampus. Notably, these influences were significantly stronger on dorsal, compared to ventral, PPC. Finally, surrogate data analysis revealed that the strength of information flow between brain areas were significantly above chance levels. Our findings provide novel insights into the integrative role of the dorsal PPC during numerical problem solving.

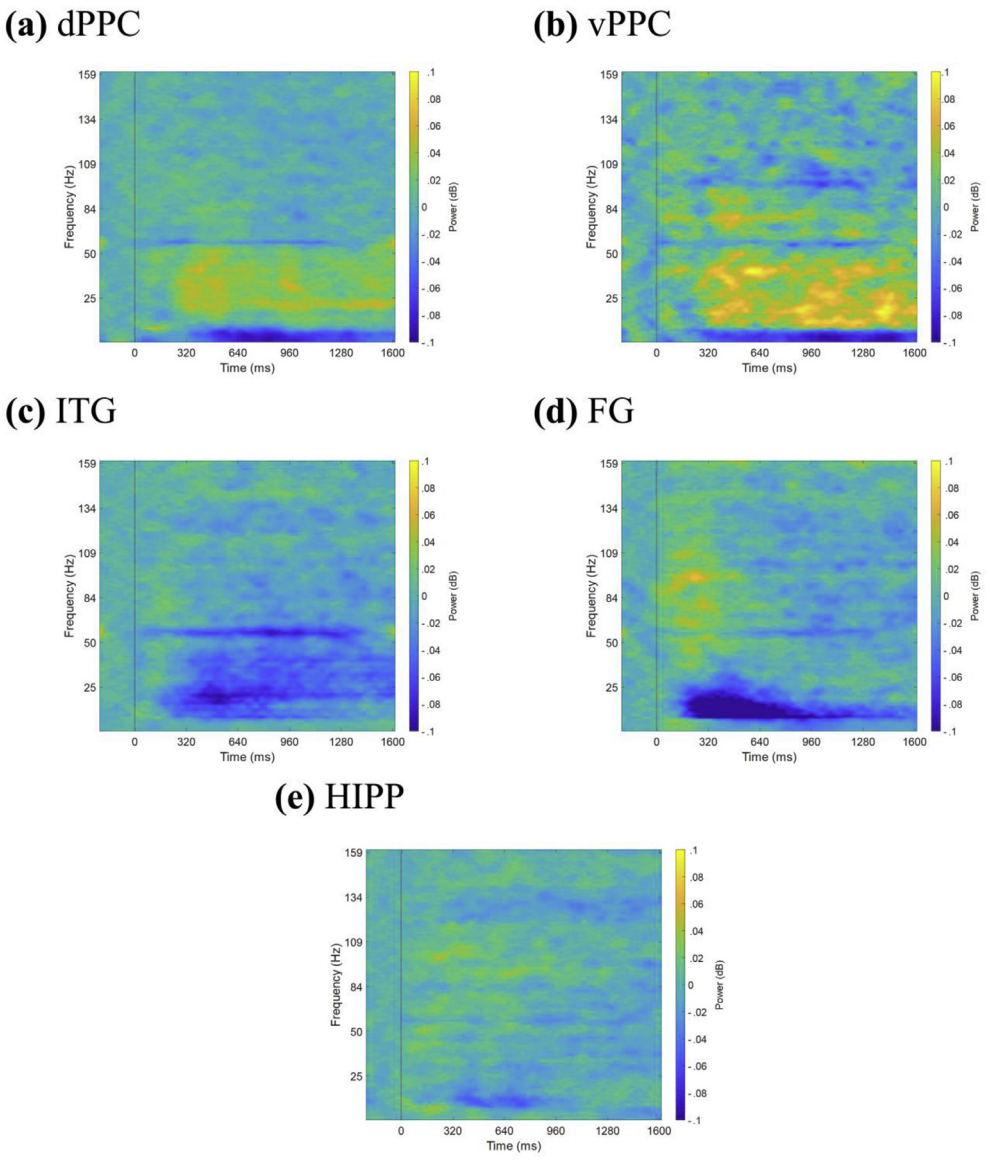

Fig. 6 – Spectrograms of iEEG activity during mental arithmetic. (a) dorsal PPC, (b) ventral PPC, (c) inferior temporal gyrus, (d) fusiform gyrus, and (e) hippocampus. Power is shown db, after normalization with pre-stimulus baseline. Line frequencies have been removed by filtering, and y-axis adjusted accordingly for visualization.

2.1. *Dorsal PPC is a dominant causal inflow hub during mental arithmetic*

The first goal of our study was to characterize causal circuits and directionality of information flow between distributed parietal and temporal cortex regions implicated in mental arithmetic (Menon et al., 2020). Our analysis focused on dorsal and ventral PPC, encompassing two distinct functional subdivisions of the parietal cortex, along with the ITG and FG subdivisions of the VTOC and the hippocampus. A key aspect of our approach is that we did not sub-select electrodes based on arbitrary thresholding of task activation or deactivation profiles, which allowed us to probe the electrophysiological basis of causal interactions between neuroanatomically-defined brain regions of interest (Fig. 1) (Fan et al., 2016) in as unbiased and general manner as possible.

To characterize the neurophysiological basis of dynamic causal interactions between brain regions, we used phase transfer entropy (PTE), which provides a robust and powerful tool for characterizing information flow between brain regions based on phase coupling (Hillebrand et al., 2016; Lobier et al., 2014; Wang et al., 2017). In an advance over Granger causal analysis and other related techniques, PTE can capture nonlinear interactions and estimate causality between nonstationary time-series, and is more accurate and computationally less expensive than transfer entropy (Barnett & Seth, 2011; Hillebrand et al., 2016; Lobier et al., 2014; Schreiber, 2000). Furthermore, PTE estimates causal

interactions based on phase coupling and is therefore insensitive to amplitude fluctuations (Barnett & Seth, 2011; Hillebrand et al., 2016; Lobier et al., 2014; Schreiber, 2000).

The dorsal PPC emerged as a causal inflow hub, characterized by net positive inflow (Fig. 2). Higher net causal inflow of the dorsal PPC relative to other parietal and temporal lobe regions during mental arithmetic is consistent with, and extends, previous reports of relatively late response onset latency of dorsal PPC compared to other brain areas during mental arithmetic (Daitch et al., 2016). The dorsal PPC also showed a stronger net causal inflow during mental arithmetic, compared to resting-state and verbal memory recall (Fig. 4a), demonstrating an enhanced role in integrating signals from other parietal and temporal cortical areas during numerical problem solving. Our findings reveal that the dPPC is a locus of feedforward signaling which links ventral temporal-occipital cortex regions involved in number processing with hippocampal regions involved in mnemonic representation of arithmetic facts.

2.2. *Information flow from ventral temporal cortex (VTOC) to dorsal PPC*

Our second goal was to probe information flow from the VTOC to the PPC. The dorsal PPC and VTOC constitute distinct functional units of the number processing system which form critical building blocks from which mathematical knowledge is constructed. Both regions play a critical role in representing non-symbolic (e.g., array of dots) and symbolic (e.g., Arabic numerals) numerical quantities. Quantity-selective neurons have been found in non-human primate PPC (Nieder, 2016) and fMRI adaptation paradigms have suggested that the PPC is sensitive to quantity across stimulus formats (Bulthé et al., 2014; Cohen Kadosh et al., 2007; Piazza et al., 2007). In contrast, the ventral temporal-occipital cortex is specialized for visual number form processing (Grotheer et al., 2016b; Hannagan et al., 2015; Piazza and Eger, 2016; Yeo et al., 2017). However, how these regions interact during numerical problem solving is poorly understood.

Both PTE analysis and surrogate analysis of causal information flow revealed that both the ITG and FG subdivisions of the VTOC had strong influences on the dorsal PPC. Both the ITG and FG, showed net positive outflow. Taken together, these findings reveal feedforward information flow from the symbolic number form processing system anchored in the VTOC to the visuospatial attention system anchored in the dorsal PPC. This pattern of directional information flow may facilitate efficient manipulation of symbolic quantities necessary for mental arithmetic (Menon, 2015). Our findings bridge an important gap in the literature and address limitations of fMRI studies which have not been able to uncover differences in information flow between brain areas crucial for number processing.

2.3. *Information flow between hippocampus and dorsal PPC*

Our next related goal was to probe causal influences of the hippocampus on the PPC. In contrast to VTOC, the role of the hippocampus in mental arithmetic has been much less studied. The importance of the medial temporal lobe, particularly its hippocampal subdivision, in verbal memory recall is well known (Squire et al., 2015). However, it is only recently that neuroimaging studies have revealed a role for the hippocampus in numerical problem solving (Bloechle et al., 2016; Moeller et al., 2015; Qin et al., 2014). Crucially, the electrophysiological correlates of hippocampal involvement and the direction of information flow to and from the hippocampus to the PPC is not known. Our study addresses an important gap in this regard by demonstrating strong information transfer from the hippocampus to the dorsal PPC.

PTE analysis revealed that the hippocampus has strong causal influences on the dorsal PPC. Moreover, net causal outflow from the hippocampus was higher than that of the ITG, but lower than that of the FG. Surprisingly, PTE analysis also revealed that, compared to both the ITG and FG subdivisions of the VTOC, the hippocampus had greater influences on the dorsal PPC (Fig. 2d).

Enhanced functional connectivity of the hippocampus with the PPC associated with memory recall has been reported in non-human primates (Miyamoto et al., 2013), and has been hypothesized to be a foundational circuit for memory recall (Vincent et al., 2006; Wagner et al., 2005). More specifically, our results converge on a recent single-neuron study that suggests that the human hippocampus plays an important role in encoding numbers (Kutter et al., 2018), and provides novel electrophysiological evidence for a causal role in mental arithmetic. Taken together, our findings provide novel electrophysiological evidence for a key role of hippocampal-parietal circuits in mental arithmetic linking the dPPC, a hub for representation and manipulation of numerical quantity, with the hippocampus, a hub for memory encoding and recall. Further studies with behavioral assessments of strategy use are needed to determine the precise contribution of this circuit to fact retrieval strategies during mental arithmetic.

2.4. *Distinct information flow associated with dorsal and ventral PPC*

Our final goal was to contrast the causal dynamics of dorsal and ventral PPC, as both regions have been implicated in fMRI studies of mental arithmetic (Grabner et al., 2009, 2013; Bloechle et al., 2016; Iuculano et al., 2018). Crucially, their differential dynamic network causal interactions have not been investigated in iEEG studies. As noted above, the net causal inflow was the strongest into dorsal PPC, relative to ventral PPC and temporal lobe regions during mental arithmetic. Notably, in contrast to dorsal PPC, the net causal inflow into ventral PPC during mental arithmetic condition did not differ from resting-state and was lower compared to verbal memory recall condition (Fig. 4b). Our results provide novel electrophysiological evidence that the dorsal PPC plays a greater role during mental arithmetic, when compared to ventral PPC. Crucially, it should be noted that we did not find significant differences in overall power between dorsal, compared to ventral, PPC, likely due to unbiased selection of electrodes in the present study. In an advance over observations of localized patterns of fMRI responses, our results further point to functional heterogeneity of subdivisions of the PPC on the basis of distinct causal dynamics unconfounded by complex patterns of activation and deactivation of

the angular gyrus in the ventral PPC observed in fMRI studies (Uddin et al., 2010). Notably, information flow into the ventral aspects of the PPC was indistinguishable from resting baseline, suggesting a weak role, if any, in mental arithmetic. The dorsal and ventral PPC were also distinguished by stronger causal influences on dorsal, compared to ventral, PPC during mental arithmetic from both the ITG and the FG subdivisions of the VTOC (Fig. 3).

Taken together, our findings reveal distinct causal dynamics of dorsal and ventral PPC both in terms of overall strength of causal influences and specific causal pathways associated with mental arithmetic, further clarifying the unique role of the dorsal PPC in integrating signals from both the VTOC and hippocampus during numerical problem solving.

2.5. *Phase transfer entropy, rather than power spectral density, and spectrograms, distinguishes causal dynamics of dorsal PPC from other brain regions and between tasks*

Phase transfer entropy (PTE) provides a robust measure of the direction of information flow between electrode pairs (Lobier et al., 2014; Lopour et al., 2013; Menon et al., 1996). PTE is based on the ability of the time-series of a brain region to predict the future values of the time-series of another by considering all possible time-points in the post-stimulus period of brain regions under consideration thus estimating the time-delayed causal influences between the two time-series. Higher PTE implies higher predictive power of one time-series from another. Previous findings using multielectrode array recordings in both humans and animal studies have suggested the crucial role of phase, rather than amplitude, modulation in information processing and signaling between brain regions (Kayser et al., 2009; Lachaux et al., 1999; Lopour et al., 2013; Ng et al., 2013; Siegel et al., 2009). In line with this view, we found significant causal influences based on phase transfer entropy, even in the absence of differences in both broadband and high-gamma power between parietal and temporal regions examined in this study. Finally, power in dorsal PPC electrodes did not differ between mental arithmetic, resting-state, and verbal memory recall conditions.

Taken together, these results suggest that the causal dynamics of dorsal PPC during mental arithmetic reflect distinct profiles of asymmetric information flow, as captured by PTE measures, rather than task-related differences in the amplitude of iEEG fluctuations.

2.6. *Theoretical implications for neurocognitive models of mental arithmetic*

Our findings inform theoretical models which have argued for a differential role for dorsal and ventral PPC in numerical cognition, and mental arithmetic in particular. Whereas the intraparietal sulcus, superior parietal lobule and supramarginal gyrus subdivisions of the dorsal PPC are thought to be involved in covert orientation along a mental number line, given its well-known role in spatial attention (Corbetta & Shulman, 2011), the angular gyrus within the ventral PPC has been linked to retrieval of arithmetic facts (Grabner et al., 2009). Furthermore, the ventral PPC and hippocampus are part of default mode network regions implicated in semantic and memory processing (Binder & Desai, 2011; Greicius et al., 2003; Schacter et al., 1996). Crucially, despite the hypothesized role of the angular gyrus in verbal fact retrieval, its functional contribution to mental arithmetic has remained elusive. In contrast to the intraparietal sulcus, superior parietal lobule and supramarginal gyrus which form part of distinct lateral frontoparietal circuits engaged during cognition, the angular gyrus is part of default mode network regions that are disengaged during cognition and are typically deactivated during mental arithmetic tasks (Ansari, 2008; Grabner et al., 2009; Menon, 2016). Given concerns that complex patterns of activation and deactivation reported in fMRI studies might be an artifact related to blood flow and oxygenation changes, it is crucial to establish neurophysiological parallels. Daitch and colleagues reported that the angular gyrus was sensitive to episodic memory recall but was relatively unchanged from baseline during mental arithmetic (Daitch et al., 2016). Convergent on these observations we found weaker causal influences from both the ITG and FG subdivisions of the VTOC on the posterior, compared to the dorsal, PPC. Moreover, the dorsal PPC also received stronger inputs from the ITG, FG and hippocampus than it did from the ventral PPC. Finally, unlike the dorsal PPC, causal influences on the ventral PPC during mental arithmetic were not differentiated from the resting-baseline. These findings further hint at a weaker role of the angular gyrus in mental arithmetic, and provide insights into the dominant integrative functions of the dorsal PPC.

Finally, an intriguing question raised by our study is how information that is integrated by the dorsal PPC is processed further. Given multiple interconnected lateral frontoparietal circuits that link the dorsal PPC with distributed prefrontal cortex networks (Menon, 2016), hubs in the dorsal PPC are well placed to facilitate interactions with frontal lobe regions subserving working memory and decision-making systems as well as motor areas that generate output. Here it is noteworthy that Vansteensel and colleagues found temporally delayed signals in motor areas relative to both occipital and parietal cortex. Further studies using multivariate analysis of electrophysiological signals to determine the precise transformations implemented by individual dorsal PPC subdivisions, as well as time-resolved analysis of directed information flow across specific stages of information processing with iEEG recordings from distributed parietal and frontal cortices are needed to clarify how information is processed and sent to other regions until output is produced.

2.7. *Generalizability and limitations*

The mental arithmetic task was performed during the retention interval of an episodic memory task, between distinct encoding and retrieval periods. This raises the question of the extent to which the pattern of causal dynamics reported in the current study during the mental arithmetic task was influenced by prior memory encoding. Given the high level of accuracy (>93%) in the multi-operand, arithmetic task, it is unlikely that participants were actively engaged in memory replay of encoded words they had viewed earlier. Moreover, our analysis revealed that net causal inflow into the dorsal PPC was significantly higher during mental arithmetic, compared to verbal memory recall and the strength of causal

influences was significantly higher on dorsal, compared to ventral, PPC from the hippocampus during mental arithmetic, when compared to verbal memory recall. These results suggest that dynamic causal processes engaged during mental arithmetic can be differentiated from memory recall. A related question here is whether memory encoding resulted in a different brain state that limits generalizability of the findings. To the best of our knowledge, the influence of prior brain states on neural representations and causal interactions has not been directly addressed in previous studies in humans. In rodents, there is emerging evidence that hippocampus can maintain multiple stable memory representations with little interference (Sheintuch et al., 2020). Evidence from optogenetic studies in rodents suggests that memory encoding can result in an engram that is silent until triggered for recall in a context-specific manner (Kitamura et al., 2017; Roy et al., 2017). Precisely how verbal memory retention in humans influences causal signaling between brain regions, including the hippocampus, remains an open question. Future iEEG studies using tasks without the potential influences of intermediate brain states and memory load is necessary to further clarify the role of the PPC and its dynamic causal interactions during mental arithmetic.

2.8. Conclusions

Our findings reveal neurophysiological circuit mechanisms by which the visual number form processing system, anchored in the ventral temporal-occipital cortex, and the declarative memory system, anchored in the hippocampus, dynamically engage the PPC during numerical problem solving. Findings highlight involvement of the hippocampus and reveal significant functional heterogeneity in the PPC, with the dorsal PPC emerging as a dominant causal inflow hub that integrates signals from both the ventral temporal cortex and the hippocampus. Our study emphasizes significant asymmetric signaling mechanisms among interacting neurocognitive processing systems.

3. Methods

We report how we determined our sample size, all data exclusions, all inclusion/exclusion criteria, whether inclusion/exclusion criteria were established prior to data analysis, all manipulations, and all measures in the study.

3.1. UPENN-RAM iEEG recordings

iEEG recordings from 102 patients shared by Kahana and colleagues at the University of Pennsylvania (UPENN) (obtained from the UPENN-RAM public data release under release ID "Release_20171012", released on 12 October, 2017) were used for analysis (Jacobs et al., 2016). iEEG recordings were downloaded from a UPENN-RAM consortium hosted data sharing archive (URL: http://memory.psych.upenn.edu/RAM). Prior to data collection, research protocols and ethical guidelines were approved by the Institutional Review Board at the participating hospitals and informed consent was obtained from the participants and guardians (Jacobs et al., 2016). Details of all the recordings sessions and data pre-processing procedures are described by Kahana and colleagues (Jacobs et al., 2016). Briefly, iEEG recordings were obtained using subdural grids (contacts placed 10 mm apart) or depth electrodes (contacts spaced 5–10 mm apart) using recording systems at each clinical site. iEEG systems included DeltaMed XlTek (Natus), Grass Telefactor, and Nihon-Kohden EEG systems. Electrodes located in brain lesions or those which corresponded to seizure onset zones or had significant interictal spiking or had broken leads, were excluded from analysis.

Anatomical localization of electrode placement was accomplished by co-registering the postoperative computed CTs with the postoperative MRIs using FSL (FMRIB (Functional MRI of the Brain) Software Library), BET (Brain Extraction Tool), and FLIRT (FMRIB Linear Image Registration Tool) software packages. Preoperative MRIs were used when postoperative MRIs were not available. The resulting contact locations were mapped to MNI space using an indirect stereotactic technique and OsiriX Imaging Software DICOM viewer package.

iEEG signals were sampled at 1,000 Hz. The two major concerns when analyzing interactions between closely spaced intracranial electrodes are volume conduction and confounding interactions with the reference electrode (Burke et al., 2013). Hence bipolar referencing was used to eliminate confounding artifacts and improve the signal-to-noise ratio of the neural signals, consistent with previous studies using UPENN-RAM iEEG data (Burke et al., 2013; Ezzyat et al., 2018). Signals recorded at individual electrodes were converted to a bipolar montage by computing the difference in signal between adjacent electrode pairs on each strip, grid, and depth electrode and the resulting bipolar signals were treated as new virtual electrodes originating from the midpoint between each contact pair. Line noise (60 Hz) and its harmonics were removed from the bipolar signals and finally, unless otherwise specified, each bipolar signal was Z-normalized by removing mean and scaling by the standard deviation. For time series filtering, we used a fourth order two-way zero phase lag Butterworth filter for all analyses.

3.2. Participant and electrode identification

We used the Brainnetome atlas (Fan et al., 2016) to demarcate parietal, inferior temporal and hippocampus regions of interest (Table 3). We first identified electrode pairs in which there were at least five patients with electrodes implanted in each pair of brain regions of interest encompassing PPC, VTOC and hippocampal regions of interest. Key PPC regions of interest included the superior parietal lobule, supramarginal gyrus, intraparietal sulcus and angular gyrus in the inferior parietal lobule, spanning its dorsal–ventral axis. The lack of sufficient number of participants and electrode pairs precluded analyses of these subdivisions separately (Table S1). We therefore combined electrodes from the superior parietal lobule, intraparietal sulcus, and supramarginal gyrus into a dorsal PPC subdivision and the angular gyrus regions into a ventral PPC subdivision (Table 3). VTOC regions of interest included its medial and lateral aspects and were demarcated into distinct subdivisions encompassing the ITG and FG, respectively. These regions include the putative number and word form areas that are sensitive to symbolic

representations of quantity (Grotheer et al., 2016a). Electrodes from left and right hemispheres of each brain region (dorsal PPC, ventral PPC, ITG, FG, and hippocampus) were pooled to obtain adequate number of electrode pairs (Table 3) across which all subsequent analyses were performed. Out of 102 individuals, data from 35 individuals, 362 electrodes, and 1727 electrode pairs were used for subsequent analysis based on electrode placement in brain regions of interest.

3.3. iEEG recordings during mental arithmetic, verbal memory recall, and resting-state conditions

35 participants performed multiple trials of a "free recall" experiment on a laptop computer. In each trial, they were first presented with a list of 12 words sequentially. After the presentation of the final word, they immediately engaged in a series of arithmetic problems (mental arithmetic condition) in the form of $a + b + c = ??$, where a, b, and c were randomly selected integers ranging from 1 to 9 (Fig. 1d). Participants were instructed to complete as many problems as possible within a ~20s time window. Participants solved an average of 52 arithmetic problems. They entered their answers via the laptop's keyboard. A new arithmetic problem was displayed on the screen as soon as the previous answer was entered. After completion of the arithmetic problem, participants were asked to recall as many words as possible for ~30 sec from the list of words that was presented just before answering arithmetic problems (verbal memory recall condition). Details of the task are described elsewhere (Solomon et al., 2017, 2019). To determine the electrophysiological properties and dynamic neural circuit mechanisms underlying successful mental arithmetic and verbal memory recall, only accurate trials from these conditions were included in our analysis. Recordings of the first 1.6 sec of each arithmetic problem were used to conduct trial-by-trial analysis of causal dynamics.

The choice of 1.6 sec duration was based on reaction time reported in behavioral and fMRI studies (Rosenberg-Lee et al., 2011) as well as iEEG (Daitch et al., 2016; Pinheiro-Chagas et al., 2018), which have shown significant event-related activity of select brain regions involved in mathematical cognition within this time window. We chose an identical 1.6 sec for each verbal memory recall trial. Resting-state data consisted of intervals prior to each encoding block in which participants were asked to fixate on the screen and alerted to the upcoming task. This choice of resting-state data is consistent with previous iEEG and fMRI studies (Das & Menon, 2020; Smith et al., 2018). Moreover, in a previous study we showed that these resting-state epochs accurately reproduced findings from conventional resting-state iEEG data acquired from an independent cohort (Das & Menon, 2020). For the resting-state condition, we extracted 10-s iEEG recordings (epochs) prior to the beginning of each trial, corresponding to the ITI. To reduce boundary and carry over effects, we discarded 3 sec at the beginning and 3 sec at the end of each epoch, resulting in 4-s epochs for resting-state condition. Resting-state related recordings were randomly selected to match their length to those from mental arithmetic/verbal memory recall periods. Each of 1.6 sec recordings (mental arithmetic/verbal memory recall/resting-state) was analyzed separately and averaged across trials to obtain relevant measures of interest.

3.4. iEEG analysis of power and time-frequency decomposition

Time-frequency analysis for mental arithmetic events were estimated using a short-time duration Fourier transformation method (Zhou et al., 2019). Spectrograms were calculated in .25s windows with 90% overlap with a Hanning window for smoothing and db-normalized with respect to .2sec pre-stimulus periods. Finally, spectrograms were averaged across time and broadband frequency range to estimate the average power for each brain region of interest (dorsal PPC, ventral PPC, ITG, FG, and HIPP). Power for resting-state and memory recall periods were calculated in a similar way after normalization with respect to .2sec periods immediately preceding the resting-state and memory recall periods respectively.

3.5. iEEG analysis of phase transfer entropy (PTE) and causal dynamics

A brain region, X, has a causal influence on a target region, Y, if knowing past signals from both regions (X and Y) improves the ability to predict the target region's (Y) future signals, in comparison to knowing only the target region's (Y) past signals (Granger, 1969; Marinazzo et al., 2008). In an advance over Granger causality analysis which is limited to assessing directionality of linear interactions and stationary time-series (Barnett & Seth, 2011), phase transfer entropy (PTE) is a robust, nonlinear measure of directionality of information flow between time-series and can be applied as a measure of causality to nonstationary time-series (Lobier et al., 2014). PTE has also been shown to be computationally more efficient than transfer entropy (TE) (Lobier et al., 2014). Our stationarity test of iEEG recordings (unit root test for stationarity) revealed that the spectral radius of the autoregressive model is very close to one, indicating that iEEG time-series is nonstationary (Barnett & Seth, 2014). We therefore used PTE (described below) to determine nonlinear, nonstationary causal dynamics observed in iEEG data in our study.

Given two time-series $\{x_i\}$ and $\{y_i\}$, where $i = 1, 2, \ldots, M$, instantaneous phases were first extracted using the Hilbert transform. Let $\{x_i^p\}$ and $\{y_i^p\}$, where $i = 1, 2, \ldots, M$, denote the corresponding phase time-series. If the uncertainty of the target signal $\{y_i^p\}$ at delay τ is quantified using Shannon entropy, then the PTE from driver signal $\{x_i^p\}$ to target signal $\{y_i^p\}$ can be given by

$$PTE_{x\to y} = \sum_i p(y_{i+\tau}^p, y_i^p, x_i^p)\log\left(\frac{p(y_{i+\tau}^p|y_i^p, x_i^p)}{p(y_{i+\tau}^p|y_i^p)}\right), \quad \text{(viii)}$$

where probabilities can be calculated by building histograms of occurrences of singles, pairs, or triplets of instantaneous phase estimates from phase time-series (Hillebrand et al., 2016). PTE is measured in *bits*, same as entropy. For our analysis, the number of bins in histograms was set as $3.49 \times STD \times M^{-1/3}$ and delay τ was set as $2M/M_{\pm}$, where STD is average standard deviation of phase time-series $\{x_i^p\}$ and $\{y_i^p\}$ and $M_{\pm}$ is the number of times the phase changes sign across time and channels (Hillebrand et al., 2016). Note that PTE is robust against the choice of the delay τ and the number of bins for forming the histograms and variations in these parameters

do not change the results much (Hillebrand et al., 2016). For PTE estimation, we used the broadband signal (.5–80 Hz) rather than the filtered signal, since causality estimation is very sensitive to filtering [see (Barnett & Seth, 2011) for a detailed discussion on this].

Net causal outflow was calculated as the difference between the total outgoing information and total incoming information, that is, net causal outflow = PTE(out) − PTE(in). For calculation of PTE(out) and PTE(in) for dorsal PPC electrodes, electrodes in the ventral PPC, ITG, FG, and HIPP were considered, that is, PTE(out) was calculated as the net PTE from dorsal PPC electrodes to the ventral PPC, ITG, FG, and HIPP electrodes, and PTE(in) was calculated as the net PTE from the ventral PPC, ITG, FG, and HIPP electrodes to dorsal PPC electrodes. PTE(out) and PTE(in) for ventral PPC, ITG, FG, and HIPP electrodes were calculated in a similar way. A brain region (for example, dorsal PPC) was defined to be a "causal inflow hub" if the net causal inflow PTE(in) − PTE(out) is the maximum among all brain regions. Similarly, a brain region was defined to be a "causal outflow hub" if the net causal outflow PTE(out) − PTE(in) is the maximum among all brain regions.

3.6. *Statistical analysis*

Statistical analysis was conducted using mixed effects analysis with the lmerTest package (Kuznetsova et al., 2017) implemented in R software (version 4.0.2, R Foundation for Statistical Computing). Because PTE data were not normally distributed, we used BestNormalize (Peterson and Cavanaugh, 2018) which contains a suite of transformation-estimating functions that can be used to optimally normalize data. The resulting normally distributed data were subjected to mixed effects analysis with the following model: *PTE ~ Condition + (1|Subject)*, where *Condition* models the fixed effects (condition differences) and (1|*Subject*) models the random repeated measurements within the same participant. Analysis of variance (ANOVA) was used to test the significance of findings with FDR-corrections for multiple comparisons ($p < .05$). Similar mixed effects statistical analysis procedures were used for comparison of power spectral density across brain regions.

Finally, we conducted surrogate analysis to test the significance of the estimated PTE values (Hillebrand et al., 2016). The estimated phases from the Hilbert transform for electrodes from a given pair of brain areas were time-shuffled so that the predictability of one time-series from another is destroyed, and PTE analysis was repeated on this shuffled data to build a distribution of surrogate PTE values against which the observed PTE was tested ($p < .05$).

Credit author statement

Anup Das: Conceptualization; Formal analysis; Investigation; Methodology; Project administration; Resources; Software; Validation; Visualization; Roles/Writing - original draft; Writing - review & editing.

Vinod Menon: Conceptualization; Funding acquisition; Investigation; Project administration; Supervision; Roles/Writing - original draft; Writing - review & editing.

Code availability

MATLAB codes used in this study can be downloaded here https://github.com/scsnl/Das_Cortex_2021.

Additional notes

No part of the study procedures or analyses was preregistered prior to the research being conducted.

Open practices

The study in this article earned an Open Data – Protected Access badge for transparent practices. Data for this study can be found at: http://memory.psych.upenn.edu/RAM.

Acknowledgements

We are grateful to members of the UPENN-RAM consortia for generously sharing their unique iEEG data. We thank Drs. Paul A. Wanda, Michael V. DePalatis, Youssef Ezzyat, Richard Betzel, and Leon A. Davis for assistance with the UPENN-RAM dataset. We thank Carlo de los Angeles for assistance with the Brainnetome atlas and Fig. 1, and Drs. Hyesang Chang and Ruizhe Liu for thoughtful feedback on the manuscript. We are also grateful to two anonymous reviewers for their valuable feedback. This research was supported by grants from the NIH (HD059205, HD094623, MH121069, and NS086085) and NSF (2024856).

Appendix

Table S1. Number of electrode pairs for key PPC regions of interest. ITG: inferior temporal gyrus, FG: fusiform gyrus, HIPP: hippocampus, IPS: intraparietal sulcus, SPL: superior parietal lobule, SMG: supramarginal gyrus.

Inter-regional pairs	Number of electrode pairs (n)	Number of participants
ITG-IPS	34	3
FG-IPS	34	3
AG-IPS	22	4
SPL-IPS	24	5
SMG-IPS	82	7
HIPP-IPS	14	4
ITG-SPL	16	1
FG-SPL	14	3
AG-SPL	7	3
SMG-SPL	54	4
HIPP-SPL	11	2
ITG-SMG	268	10
FG-SMG	94	7
AG-SMG	177	9
HIPP-SMG	95	10

REFERENCES

Ansari, D. (2008). Effects of development and enculturation on number representation in the brain. *Nature Reviews. Neuroscience, 9*, 278–291.

Barnett, L., & Seth, A. K. (2011). Behaviour of Granger causality under filtering: Theoretical invariance and practical application. *Journal of Neuroscience Methods, 201*, 404–419.

Barnett, L., & Seth, A. K. (2014). The MVGC multivariate granger causality toolbox: A new approach to granger-causal inference. *Journal of Neuroscience Methods, 223*, 50–68.

Binder, J. R., & Desai, R. H. (2011). The neurobiology of semantic memory. *Trends in Cognitive Sciences, 15*, 527–536.

Bloechle, J., Huber, S., Bahnmueller, J., Rennig, J., Willmes, K., Cavdaroglu, S., Moeller, K., & Klein, E. (2016). Fact learning in complex arithmetic-the role of the angular gyrus revisited. *Human Brain Mapping, 37*, 3061–3079.

Bulthé, J., De Smedt, B., & Op de Beeck, H. P. (2014). Format-dependent representations of symbolic and non-symbolic numbers in the human cortex as revealed by multi-voxel pattern analyses. *Neuroimage, 87*, 311–322.

Burke, J. F., Zaghloul, K. A., Jacobs, J., Williams, R. B., Sperling, M. R., Sharan, A. D., & Kahana, M. J. (2013). Synchronous and asynchronous theta and gamma activity during episodic memory formation. *The Journal of Neuroscience: the Official Journal of the Society for Neuroscience, 33*, 292–304.

Canolty, R. T., & Knight, R. T. (2010). The functional role of cross-frequency coupling. *Trends in Cognitive Sciences, 14*, 506–515.

Chang, H., Rosenberg-Lee, M., Qin, S., & Menon, V. (2019). Faster learners transfer their knowledge better: Behavioral, mnemonic, and neural mechanisms of individual differences in children's learning. *Developmental Cognitive Neuroscience, 40*, 100719.

Cho, S., Metcalfe, A. W., Young, C. B., Ryali, S., Geary, D. C., & Menon, V. (2012). Hippocampal-prefrontal engagement and dynamic causal interactions in the maturation of children's fact retrieval. *Journal of Cognitive Neuroscience, 24*, 1849–1866.

Cohen Kadosh, R., Cohen Kadosh, K., Kaas, A., Henik, A., & Goebel, R. (2007). Notation-dependent and -independent representations of numbers in the parietal lobes. *Neuron, 53*, 307–314.

Corbetta, M., & Shulman, G. L. (2011). Spatial neglect and attention networks. *Annual Review of Neuroscience, 34*, 569–599.

Daitch, A. L., Foster, B. L., Schrouff, J., Rangarajan, V., Kaşikçi, I., Gattas, S., & Parvizi, J. (2016). Mapping human temporal and parietal neuronal population activity and functional coupling during mathematical cognition. *Proceedings of the National Academy of Sciences, 113*, E7277–E7286.

Das, A., & Menon, V. (2020). Spatiotemporal integrity and spontaneous nonlinear dynamic properties of the salience network revealed by human intracranial electrophysiology: A multicohort replication. *Cerebral Cortex, 30*, 5309–5321.

Dastjerdi, M., Ozker, M., Foster, B. L., Rangarajan, V., & Parvizi, J. (2013). Numerical processing in the human parietal cortex during experimental and natural conditions. *Nature Communications, 4*, 2528.

Dehaene, S., Piazza, M., Pinel, P., & Cohen, L. (2003). Three parietal circuits for number processing. *Cognitive Neuropsychology, 20*, 487–506.

Ezzyat, Y., Wanda, P. A., Levy, D. F., Kadel, A., Aka, A., Pedisich, I., Sperling, M. R., Sharan, A. D., Lega, B. C., Burks, A., & Gross, R. E. (2018). Closed-loop stimulation of temporal cortex rescues functional networks and improves memory. *Nature Communications, 9*, 365.

Fan, L., Li, H., Zhuo, J., Zhang, Y., Wang, J., Chen, L., Yang, Z., Chu, C., Xie, S., Laird, A. R., Fox, P. T., Eickhoff, S. B., Yu, C., & Jiang, T. (2016). The human brainnetome atlas: A new brain atlas based on connectional architecture. *Cerebral Cortex, 26*, 3508–3526.

Fias, W., Menon, V., & Szucs, D. (2013). Multiple components of developmental dyscalculia. *Trends in Neuroscience and Education, 2*, 43–47.

Grabner, R. H., Ansari, D., Koschutnig, K., Reishofer, G., & Ebner, F. (2013). The function of the left angular gyrus in mental arithmetic: Evidence from the associative confusion effect. *Human Brain Mapping, 34*, 1013–1024.

Grabner, R. H., Ansari, D., Koschutnig, K., Reishofer, G., Ebner, F., & Neuper, C. (2009). To retrieve or to calculate? Left angular gyrus mediates the retrieval of arithmetic facts during problem solving. *Neuropsychologia, 47*, 604–608.

Granger, C. W. J. (1969). Investigating causal relations by econometric models and cross-spectral methods. *Econometrica, 37*, 424–438.

Greicius, M. D., Krasnow, B., Reiss, A. L., & Menon, V. (2003). Functional connectivity in the resting brain: A network analysis of the default mode hypothesis. *Proceedings of the National Academy of Sciences, 100*, 253–258.

Grotheer, M., Ambrus, G. G., & Kovacs, G. (2016b). Causal evidence of the involvement of the number form area in the visual detection of numbers and letters. *Neuroimage, 132*, 314–319.

Grotheer, M., Herrmann, K. H., & Kovács, G. (2016a). Neuroimaging evidence of a bilateral representation for visually presented numbers. *The Journal of Neuroscience: the Official Journal of the Society for Neuroscience, 36*, 88–97.

Hannagan, T., Amedi, A., Cohen, L., Dehaene-Lambertz, G., & Dehaene, S. (2015). Origins of the specialization for letters and numbers in ventral occipitotemporal cortex. *Trends in Cognitive Sciences, 19*, 374–382.

Hermes, D., Rangarajan, V., Foster, B. L., King, J. R., Kasikci, I., Miller, K. J., & Parvizi, J. (2017). Electrophysiological responses in the ventral temporal cortex during reading of numerals and calculation. *Cerebral Cortex, 27*, 567–575.

Hillebrand, A., Tewarie, P., van Dellen, E., Yu, M., Carbo, E. W., Douw, L., Gouw, A. A., van Straaten, E. C., & Stam, C. J. (2016). Direction of information flow in large-scale resting-state networks is frequency-dependent. *Proceedings of the National Academy of Sciences, 113*, 3867–3872.

Iuculano, T., & Menon, V. (2018). Development of mathematical reasoning. In S. Ghetti (Ed.), *Stevens' handbook of experimental psychology and cognitive neuroscience*. John Wiley & Sons.

Iuculano, T., Padmanabhan, A., & Menon, V. (2018). Systems neuroscience of mathematical cognition and learning: Basic organization and neural sources of heterogeneity in typical and atypical development. In A. Henik, & W. Fias (Eds.), *Heterogeneity of function in numerical cognition* (pp. 287–336). Waltham: Academic Press.

Jacobs, J., Miller, J., Lee, S. A., Coffey, T., Watrous, A. J., Sperling, M. R., Sharan, A., Worrell, G., Berry, B., Lega, B., Jobst, B. C., Davis, K., Gross, R. E., Sheth, S. A., Ezzyat, Y., Das, S. R., Stein, J., Gorniak, R., Kahana, M. J., & Rizzuto, D. S. (2016). Direct electrical stimulation of the human entorhinal region and Hippocampus impairs memory. *Neuron, 92*, 983–990.

Jolles, D., Supekar, K., Richardson, J., Tenison, C., Ashkenazi, S., Rosenberg-Lee, M., Fuchs, L., & Menon, V. (2016). Reconfiguration of parietal circuits with cognitive tutoring in elementary school children. *Cortex; a Journal Devoted To the Study of the Nervous System and Behavior, 83*, 231–245.

Kayser, C., Montemurro, M. A., Logothetis, N. K., & Panzeri, S. (2009). Spike-phase coding boosts and stabilizes information carried by spatial and temporal spike patterns. *Neuron, 61*, 597–608.

Kitamura, T., Ogawa, S. K., Roy, D. S., Okuyama, T., Morrissey, M. D., Smith, L. M., Redondo, R. L., & Tonegawa, S. (2017). Engrams and circuits crucial for systems consolidation of a memory. *Science, 356*, 73–78.

Kucian, K., & von Aster, M. (2015). Developmental dyscalculia. *European Journal of Pediatrics, 174*, 1–13.

Kutter, E. F., Bostroem, J., Elger, C. E., Mormann, F., & Nieder, A. (2018). Single neurons in the human brain encode numbers. *Neuron, 100*, 753–761. e754.
Kuznetsova, A., Brockhoff, P. B., & Christensen, R. H. B. (2017). lmerTest package: Tests in linear mixed effects models. *Journal of Cognitive Neuroscience, 82*, 1–26.
Lachaux, J. P., Rodriguez, E., Martinerie, J., & Varela, F. J. (1999). Measuring phase synchrony in brain signals. *Human Brain Mapping, 8*, 194–208.
Lobier, M., Siebenhühner, F., Palva, S., & Matias, P. J. (2014). Phase transfer entropy: A novel phase-based measure for directed connectivity in networks coupled by oscillatory interactions. *Neuroimage, 85*, 853–872.
Lopour, B. A., Tavassoli, A., Fried, I., & Ringach, D. L. (2013). Coding of information in the phase of local field potentials within human medial temporal lobe. *Neuron, 79*, 594–606.
Marinazzo, D., Pellicoro, M., & Stramaglia, S. (2008). Kernel method for nonlinear granger causality. *Physical Review Letters, 100*, 144103.
Mathieu, R., Epinat-Duclos, J., Léone, J., Fayol, M., Thevenot, C., & Prado, J. (2018). Hippocampal spatial mechanisms relate to the development of arithmetic symbol processing in children. *Developmental Cognitive Neuroscience, 30*, 324–332.
Menon, V. (2015). Arithmetic in the child and adult brain. In R. C. Kadosh, & A. Dowker (Eds.), *The oxford handbook of numerical cognition*. Oxford: Oxford University Press.
Menon, V. (2016). Memory and cognitive control circuits in mathematical cognition and learning. *Progress in Brain Research, 227*, 159–186.
Menon, V., Freeman, W. J., Cutillo, B. A., Desmond, J. E., Ward, M. F., Bressler, S. L., Laxer, K. D., Barbaro, N., & Gevins, A. S. (1996). Spatio-temporal correlations in human gamma band electrocorticograms. *Electroencephalography and Clinical Neurophysiology, 98*, 89–102.
Menon, V., Padmanabhan, A., & Schwartz, F. (2020). Cognitive neuroscience of dyscalculia and math learning disabilities. In K. C. Kadosh (Ed.), *The oxford handbook of developmental cognitive neuroscience*. Oxford: Oxford University Press.
Miyamoto, K., Osada, T., Adachi, Y., Matsui, T., Kimura, H. M., & Miyashita, Y. (2013). Functional differentiation of memory retrieval network in macaque posterior parietal cortex. *Neuron, 77*, 787–799.
Moeller, K., Willmes, K., & Klein, E. (2015). A review on functional and structural brain connectivity in numerical cognition. *Frontiers in Human Neuroscience, 9*, 227.
Ng, B. S., Logothetis, N. K., & Kayser, C. (2013). EEG phase patterns reflect the selectivity of neural firing. *Cerebral Cortex, 23*, 389–398.
Nieder, A. (2016). The neuronal code for number. *Nature Reviews. Neuroscience, 17*, 366–382.
Park, J., Park, D. C., & Polk, T. A. (2013). Parietal functional connectivity in numerical cognition. *Cerebral Cortex, 23*, 2127–2135.
Peters, L., & De Smedt, B. (2018). Arithmetic in the developing brain: A review of brain imaging studies. *Developmental Cognitive Neuroscience, 30*, 265–279.
Peterson, R. A., & Cavanaugh, J. E. (2018). Ordered quantile normalization: A semiparametric transformation built for the cross-validation era. *Journal of Cognitive Neuroscience, 82*, 2312–2327.
Piazza, M., & Eger, E. (2016). Neural foundations and functional specificity of number representations. *Neuropsychologia, 83*, 257–273.
Piazza, M., Pinel, P., Le Bihan, D., & Dehaene, S. (2007). A magnitude code common to numerosities and number symbols in human intraparietal cortex. *Neuron, 53*, 293–305.
Pinheiro-Chagas, P., Daitch, A., Parvizi, J., & Dehaene, S. (2018). Brain mechanisms of arithmetic: A crucial role for ventral temporal cortex. *Journal of Cognitive Neuroscience, 30*, 1757–1772.
Qin, S., Cho, S., Chen, T., Rosenberg-Lee, M., Geary, D. C., & Menon, V. (2014). Hippocampal-neocortical functional reorganization underlies children's cognitive development. *Nature Neuroscience, 17*, 1263–1269.
Rosenberg-Lee, M., Chang, T. T., Young, C. B., Wu, S., & Menon, V. (2011). Functional dissociations between four basic arithmetic operations in the human posterior parietal cortex: A cytoarchitectonic mapping study. *Neuropsychologia, 49*, 2592–2608.
Rosenberg-Lee, M., Iuculano, T., Bae, S. R., Richardson, J., Qin, S., Jolles, D., & Menon, V. (2017). Short-term cognitive training recapitulates hippocampal functional changes associated with one year of longitudinal skill development. *Trends in Neuroscience and Education, 10*, 19–29.
Roy, D. S., Muralidhar, S., Smith, L. M., & Tonegawa, S. (2017). Silent memory engrams as the basis for retrograde amnesia. *Proceedings of the National Academy of Sciences, 114*, E9972–E9979.
Schacter, D. L., Alpert, N. M., Savage, C. R., Rauch, S. L., & Albert, M. S. (1996). Conscious recollection and the human hippocampal formation: Evidence from positron emission tomography. *Proceedings of the National Academy of Sciences, 93*, 321–325.
Schölvinck, M. L., Maier, A., Ye, F. Q., Duyn, J. H., & Leopold, D. A. (2010). Neural basis of global resting-state fMRI activity. *Proceedings of the National Academy of Sciences, 107*, 10238–10243.
Schreiber, T. (2000). Measuring information transfer. *Physical Review Letters, 85*, 461–464.
Sheintuch, L., Geva, N., Baumer, H., Rechavi, Y., Rubin, A., & Ziv, Y. (2020). Multiple maps of the same spatial context can stably coexist in the mouse Hippocampus. *Current Biology: CB, 30*, 1467–1476. e1466.
Siegel, M., Warden, M. R., & Miller, E. K. (2009). Phase-dependent neuronal coding of objects in short-term memory. *Proceedings of the National Academy of Sciences, 106*, 21341–21346.
Smith, V., Mitchell, D. J., & Duncan, J. (2018). Role of the default mode network in cognitive transitions. *Cerebral Cortex, 28*, 3685–3696.
Solomon, E. A., Kragel, J. E., Sperling, M. R., Sharan, A., Worrell, G., Kucewicz, M., Inman, C. S., Lega, B., Davis, K. A., Stein, J. M., Jobst, B. C., Zaghloul, K. A., Sheth, S. A., Rizzuto, D. S., & Kahana, M. J. (2017). Widespread theta synchrony and high-frequency desynchronization underlies enhanced cognition. *Nature Communications, 8*, 1704.
Solomon, E. A., Stein, J. M., Das, S., Gorniak, R., Sperling, M. R., Worrell, G., Inman, C. S., Tan, R. J., Jobst, B. C., Rizzuto, D. S., & Kahana, M. J. (2019). Dynamic theta networks in the human medial temporal lobe support episodic memory. *Current Biology: CB, 29*, 1100–1111. e1104.
Squire, L. R., Genzel, L., Wixted, J. T., & Morris, R. G. (2015). Memory consolidation. *Cold Spring Harbor Perspectives in Biology Electronic Resource, 7*, a021766.
Supekar, K., Swigart, A. G., Tenison, C., Jolles, D. D., Rosenberg-Lee, M., Fuchs, L., & Menon, V. (2013). Neural predictors of individual differences in response to math tutoring in primary-grade school children. *Proceedings of the National Academy of Sciences, 110*, 8230–8235.
Uddin, L. Q., Supekar, K., Amin, H., Rykhlevskaia, E., Nguyen, D. A., Greicius, M. D., & Menon, V. (2010). Dissociable connectivity within human angular gyrus and intraparietal sulcus: Evidence from functional and structural connectivity. *Cerebral Cortex, 20*, 2636–2646.
Vansteensel, M. J., Bleichner, M. G., Freudenburg, Z. V., Hermes, D., Aarnoutse, E. J., Leijten, F. S., Ferrier, C. H., Jansma, J. M., & Ramsey, N. F. (2014). Spatiotemporal

characteristics of electrocortical brain activity during mental calculation. *Human Brain Mapping, 35*, 5903–5920.
Vincent, J. L., Snyder, A. Z., Fox, M. D., Shannon, B. J., Andrews, J. R., Raichle, M. E., & Buckner, R. L. (2006). Coherent spontaneous activity identifies a hippocampal-parietal memory network. *Journal of Neurophysiology, 96*, 3517–3531.
Wagner, A. D., Shannon, B. J., Kahn, I., & Buckner, R. L. (2005). Parietal lobe contributions to episodic memory retrieval. *Trends in Cognitive Sciences, 9*, 445–453.
Wang, M. Y., Wang, J., Zhou, J., Guan, Y. G., Zhai, F., Liu, C. Q., Xu, F. F., Han, Y. X., Yan, Z. F., & Luan, G. M. (2017). Identification of the epileptogenic zone of temporal lobe epilepsy from stereo-electroencephalography signals: A phase transfer entropy and graph theory approach. *Neuroimage Clinical, 16*, 184–195.
Yeo, D. J., Wilkey, E. D., & Price, G. R. (2017). The search for the number form area: A functional neuroimaging meta-analysis. *Neuroscience and Biobehavioral Reviews, 78*, 145–160.
Zhou, Y., Sheremet, A., Qin, Y., Kennedy, J. P., DiCola, N. M., Burke, S. N., & Maurer, A. P. (2019). Methodological considerations on the use of different spectral decomposition algorithms to study hippocampal rhythms. *eNeuro, 6*.